SIMULATION TOOL FOR HYPER-SPECTRAL IMAGING FROM A SATELLITE

Monica Lapadatu, Sivert Bakken, Mariusz E. Grøtte, Morten Alver, Tor A. Johansen

Center for Autonomous Marine Operations and Systems
Department of Engineering Cybernetics
Norwegian University of Science and Technology (NTNU)
Trondheim, Norway

ABSTRACT

This paper presents a tool created for simulating the expected radiance from oceanic geophysical parameters through the atmosphere as perceived by a hyperspectral remote sensing satellite. The effects of varying off-nadir viewing angles, solar zenith angles and the presence of water clouds on the resulting radiance has been analyzed, and simulated top-of-atmosphere (TOA) radiance values coincide well with experimental data.

***Index Terms*—** Simulation, hyperspectral, satellite, ocean color, radiative transfer.

1. INTRODUCTION

Ocean color remote sensing satellites are currently being used for maritime observation and surveillance, e.g. monitoring of phytoplankton, zooplankton, river plumes, oil spills, harmful algal blooms, water sediments and ice. Past and present operational satellites are mainly concerned with multispectral data, but hyperspectral sensors are being considered more frequently for upcoming missions [1, 2]. By utilizing hyperspectral sensors it is expected to enhance the capabilities to detect targets of interest and estimate their characteristics [3]. Experimental space-based hyperspectral sensors include HICO and Hyperion [4, 5].

This paper focuses on the simulation of TOA radiance as perceived by a hyperspectral sensor in Low Earth Orbit, as well as simulation of water leaving radiance at the ocean surface.

The objective is to analyze different scenarios with varying off-nadir viewing angles, solar zenith angles and the presence of water clouds. As an alternative to existing remote sensing tools, e,g. SeaDas, SNAP and Ocean Virtual Laboratory, that use real satellite data, the simulation tool uses output data from the coupled physical and ecological ocean model SINMOD to calculate the resulting spectral response in radiance. Further, estimated atmospheric effects at TOA are added. The result is the hyperspectral image cube sensed at TOA.

The simulation tool is intended to be used for feasibility and analytical studies during the space mission design phase, as well as improve the mission operations of a possibly custom-designed hyperspectral imaging satellite that is configured to observe specific targets. This includes design and validation of the hyperspectral instrument, spacecraft attitude control during imaging, data processing algorithms and data products.

The common way to simulate geophysical variables in the ocean as hyperspectral radiance received by a satellite sensor is to combine the underwater radiative transfer code HydroLight and the atmospheric code MODTRAN [6]. Both Hydrolight and MODTRAN are commercial software, and they are not designed to work together.

Via PlanarRad and COART, open-source alternatives, a system of lookup tables were computed to make the simulation process more time effective. A temporal sensitivity of data acquisition analysis was performed, and a user friendly interface for radiance simulation was developed.

The theory is based on [6], i.e. ocean optics, which regards light and radiometry, optical oceanography, absorption, scattering, optical constituents of the ocean, radiative transfer theory, remote sensing, atmospheric effects and the bidirectional reflection distribution function.

2. SYSTEM OVERVIEW

The simulation tool is intended to support the utilization of a hyperspectral imager, as described in [7]. Furthermore, a dataset, titled the SINMOD data, is utilized in combination with the program PlanarRad in order to calculate water leaving radiance from the ocean surface. The radiance due to atmospheric effects is calculated utilizing the program COART. Combining the two results in the hyperspectral radiance at TOA.

2.1. The SINMOD data

SINMOD is an ocean model developed by SINTEF [8, 9]. It is based on the primitive Navier-Stokes equations and uses a regular horizontal grid and z-layers. High resolution simulations are achieved using a nesting scheme where larger scale simulations provide outer boundary conditions for higher resolution simulations. The top level domain covers the Norwegian Sea and Arctic Ocean in 20 km horizontal resolution, and the resolution is increased by a factor of 5 through each nesting step. The model forcing includes atmospheric reanalysis data from Era Interim [10] and climatological freshwater runoff data. Tidal dynamics are applied on the outer boundaries of the top level domain, based on 8 tidal components from TPXO [11].

The model calculates physical oceanographic variables such as surface elevation, current speed, temperature and salinity. The ecological model additionally estimates nutrient concentrations (nitrate, silicate, ammonium), phytoplankton (diatoms and flagellates), zooplankton (*Calanus finmarchicus* and *C. glacialis*) and variables such as heterotrophic nanoflagellates, microzooplankton, and fast and slow sinking detritus.

2.2. PlanarRad

PlanarRad is a free open source code for modelling light in natural waters or other homogeneous scattering and absorbing media [12].

PlanarRad produces nearly identical results to HydroLight [13]. PlanarRad is a C++ implementation of the invariant embedded numerical integration technique for calculating radiative transfer in plane-parallel media with an opaque bottom boundary [12]. It is based on the algorithm described in [6].

2.3. COART

Coupled Ocean and Atmosphere Radiative Transfer (COART) is a tool provided by NASA. The tool is able to calculate and simulate radiance and irradiance at any levels in the atmosphere and ocean.

The COART model was based on the Coupled Discrete Ordinate Radiative Transfer (CDISORT) code, which was developed from DISORT. DISORT is a publicly distributed software for radiative transfer, provided by NASA [14].

2.4. Lookup tables

Several lookup tables were created with the purpose of saving computational time for the calculation of water leaving radiance at the ocean surface. The lookup tables are especially relevant for computation of whole scenes instead of invidual pixels. MATLAB and PlanarRad were utilized in order to compute the lookup tables. MATLAB was utilized to read the chl_a concentration values from the SINMOD dataset and calculate the absorption, attenuation and scattering for the PlanarRad input files. PlanarRad calculated the water leaving radiance for the selected chl_a concentration values.

2.5. Temporal sensitivity of data acquisition analysis

A lookup table was utilized together with MATLAB in order to perform a temporal sensitivity of data acquisition analysis. The objective was to acquire a understanding of the water leaving radiance variation with regard to time. The analysis was performed by identifying several consecutive time frames from the SINMOD dataset with variation in the chl_a concentration values. The water leaving radiance was calculated for the specified values. The analysis was performed for time periods of one hour, five hours and ten hours.

2.6. Software

A software program is developed in order to make the calculation and computation of water leaving radiance just above the ocean surface given chl_a concentration, as well as of radiance at TOA due to atmospheric effects, less complicated and more rapid.

The main program is a MATLAB R2018b script. The utilized data was generated by PlanarRad, as well as a Python 2.7.12 interface for running PlanarRad in batches, initially developed by Daniel Marrable. Neither PlanarRad nor the python interface are necessary for utilizing the program, which exists in five versions. Several of the versions require the SINMOD dataset to be available. The program generates, depending on the selected version, the resulting water leaving radiance or the resulting radiance at TOA. One version of the program assumes the user is specifying the chl_a concentration values of interest. Another assumes the user is also specifying the viewing zenith or azimuth angle of interest. The third version assumes the user is specifying which geographical area and time frame from the SINMOD dataset should be utilized to obtain the chl_a concentration values. The radiance at TOA due to atmospheric effects can be computed. The final version is presenting and plotting water leaving radiance resulting from different solar zenith and azimuth angles, as well as different viewing zenith and azimuth angles.

Regardless of which version is utilized the wavelengths are defined as 400 - 800 [nm]. The chl_a concentration values must be in the range of 0.0 to 1.8 [mg chl_a m^{-3}].

3. RESULTS

The case study considers a hyperspectral imager with spectral range of 400 - 800 nm and spectral resolution of 5 nm [7].

The utilized SINMOD data consists of approximately one month of recorded data with a temporal resolution of 1 hour, produced from model domain covering the areas outside of Mid Norway, including Hitra, Frøya, Froan and Frohavet in 160 m horizontal resolution. The surface layer thickness is 3 m on average, but varies with surface elevation. The variables included are temperature [°C], chlorophyll in the surface layer [$mg\ chl\_a\ m^{-3}$], chlorophyll integrated over 0 - 50 meter per square metre [$mg\ chl\_a\ m^{-2}$], and the concentration of diatoms [$mmol\ N\ m^{-3}$] and flagellates [$mmol\ N\ m^{-3}$] in the surface layer.

Viewing zenith angles are defined differently by PlanarRad, as presented in [15], and COART, as presented in [16].

COART was prescribed to calculate radiances [$W\ m^{-2}\ \mu m^{-1}\ sr^{-1}$] at multiple wavelengths from 0.4 [μm] to 0.8 [μm]. The output, presented at TOA and at the ocean surface, represent only the radiances due to atmospheric effects.

The utilized solar zenith angle was 60°. The trace gas amounts of CO_2 and CH_4 values were set as recommended by COART. The MODTRAN maritime model was utilized as the mixed layer aerosol, while the stratospheric aerosol was set to utilize a background model. The aerosol loading was specified by the aerosol optical thickness at 0.5 [μm] of 0.2. The depth was set to 0 meters, with a bottom albedo of 0. Modelling a black surface prevents the COART outputs to include values of reflected radiance from the ocean surface.

3.1. Solar azimuth angles

The sun zenith angle was 20°. The resulting water leaving radiance values were obtained from the viewing azimuth angle of 0° and the viewing zenith angle of 170°. The angles are defined as in PlanarRad.

The water leaving radiance resulting from solar azimuth angle of 120° and 180° are roughly the same. The same holds for the water leaving radiance resulting from solar azimuth angles of 60° and 0°. The water leaving radiance resulting from the solar azimuth angle of 180° is higher than the water leaving radiance resulting from the solar azimuth angle of 60°.

3.2. Solar zenith angles

PlanarRad utilized a solar azimuth angle of 0°. The resulting water leaving radiance at the ocean surface was retrieved with the viewing azimuth angle 0° and the viewing zenith angle 170°.

COART utilized the previously presented inputs. The viewing zenith angle was 20°, while the viewing azimuth angle was 0°. The results were, after calculating the reflected radiance from the surface to TOA, the radiance due to atmospheric effects [$W\ m^{-2}\ \mu m^{-1}\ sr^{1}$] at the ocean surface and at TOA.

There is a small difference, of approximately 1-1.5 $W\ m^{-2}\ \mu m^{-1}\ sr^{-1}$, between the resulting radiance due to atmospheric effects at the ocean surface with regard to the solar zenith angles 20°, 40° and 60°. The radiance resulting from the solar zenith angle of

80° varies less with regard to wavelength, and is lower between the wavelengths 400 [nm] and 750 [nm].

The radiance at TOA resulting from the solar zenith angle of 80° differs from the radiance resulting from the other three solar zenith angles, by being lower for the wavelengths 400 - 700 [nm]. The radiance resulting from the solar zenith angle of 80° varies less with regard to wavelength than the resulting radiance from the other three solar zenith angles, as presented in figure 1.

The resulting water leaving radiance at the ocean surface with regard to various solar zenith angles differ from each other between 460 nm and 600 nm. The resulting water leaving radiance due to various solar azimuth angles differ from each other for all wavelengths. It can be inferred that the resulting water leaving radiance varies more with regard to solar azimuth angle than with solar zenith angle.

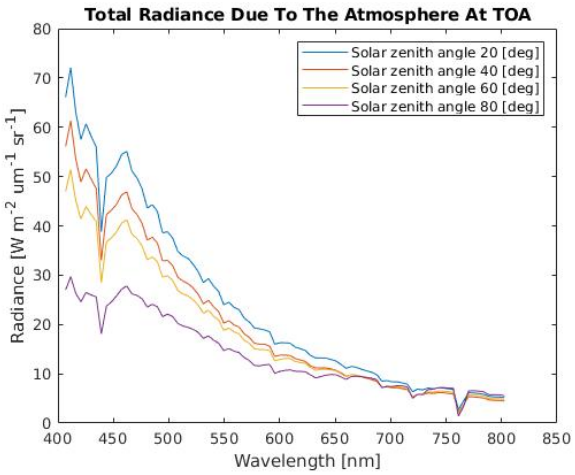

Fig. 1.

Radiance at TOA due to atmospheric effects, with regard to solar zenith angles.

3.3. Viewing azimuth angles

PlanarRad utilized the viewing zenith angle 130°, the solar azimuth angle 0° and the solar zenith angle 40°.

The test performed by COART was executed with the inputs as previously presented, and with the viewing zenith angle 20° and the viewing azimuth angle at every 60° from 0° to 180°.

The resulting radiance, both at the ocean surface and at TOA, due to atmospheric effects is roughly the same, regardless of viewing azimuth angle. See figure 2. The viewing azimuth angle resulting radiance does not vary as much as the viewing zenith angle resulting radiance.

The viewing azimuth angles of 60°, 120° and 180° result in roughly the same water leaving radiance, while the viewing azimuth angle of 0° differs from these by resulting in a water leaving radiance that is higher with approximately 0.055 sr^{-1}. Of the viewing azimuth angles of 60°, 120° and 180°, the angle 180° results in the highest water leaving radiance, while the angle 120° results in the smallest. The difference is approximately $2{\cdot}10^{-6}$ [sr^{-1}].

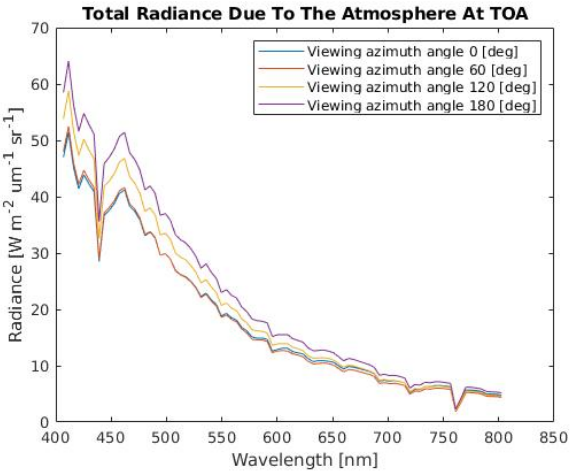

Fig. 2.

Radiance due to atmospheric effects at TOA, with regard to viewing azimuth angles.

3.4. Viewing zenith angles

PlanarRad utilized the viewing azimuth angle 0°, the solar azimuth angle 0° and the solar zenith angle 40°. The test performed by COART was executed with the azimuth and zenith radiance output angles of 0° and every 30° from 0° to 90°, respectively.

The radiance due to atmospheric effects at the ocean surface resulting from the viewing zenith angle of 60° is higher than the resulting radiances from the angles of 30° and 0°, with approximately 0.011 $W\ m^{-2}\ \mu m^{-1}\ sr^{-1}$. Likewise, the resulting radiance due to atmospheric effects at TOA from the viewing zenith angle of 60° is higher than the resulting radiances from the viewing zenith angles of 30° and 0°, with approximately 50 $W\ m^{-2}\ \mu m^{-1}\ sr^{-1}$. This is presented in figure 3.

There resulting water leaving radiance values at the ocean surface differ with regard to viewing zenith angles. The utilized angles are 120°, 150° and 170°. The viewing zenith angle of 170° results in the lowest water leaving radiance, while the angle of 150° results in the highest. The resulting water leaving radiance varies roughly the same with regard to variation in the viewing zenith angle as with regard to variation in viewing azimuth angle.

3.5. Clouds

COART was utilized to perform a test regarding the presence of water clouds. The spheric water clouds were specified to be from 3 km to 4 km of the size 10 RE [μm] and 200 liquid water path [g/m].

Figure 4 presents the impact of water clouds on the radiance at TOA due to atmospheric effects. The resulting radiance is higher

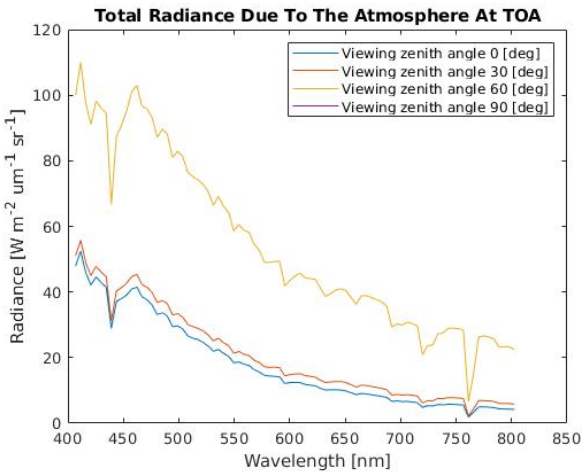

Fig. 3.

Radiance due to atmospheric effects at TOA, with regard to viewing zenith angles.

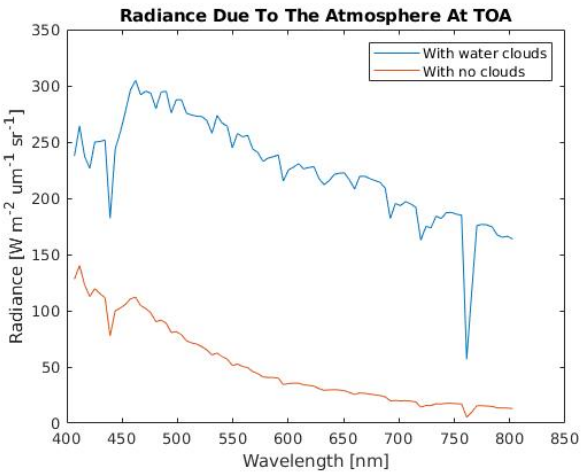

Fig. 4.

Radiance due to atmospheric effects at TOA, with regard to water clouds.

when water clouds are present than when no clouds are present, with approximately 200 $W\ m^{-2}\ \mu m^{-1}\ sr^{-1}$.

3.6. Lookup tables

The resulting water leaving radiance is identical regardless of whether it is computed by PlanarRad or by the lookup table. This suggests the lookup table works as intended. Figure 5 presents several water leaving radiance values calculated by the lookup table together with several water leaving radiance values calculated by PlanarRad. The lookup table resulting water leaving radiance values fit perfectly and follow the same wavelength dependent variations as the resulting water leaving radiance values from PlanarRad.

3.7. Temporal sensitivity of data acquisition analysis

The temporal sensitivity analysis for the time period of one hour revealed that generally the water leaving radiance varies with $0 - 0.0025\%$, and with approximately 0.015% for certain data points. The temporal sensitivity analysis for the time period of five hours revealed that generally the water leaving radiance varies with $0 - 0.02\%$, and with approximately 0.06% for certain data points. The water leaving radiance variation over the period of ten hours varies from four to eight times more than the variation over the period of one hour. The longer the time period, the bigger the water leaving radiance variation.

4. FUTURE WORK

Suggested further work includes examining how different parameters in the water body, such as ocean state and depth, affect the water leaving radiance. Examining how the camera specifications affects the recorded radiance is also of interest.

5. CONCLUSIONS

The simulation tool can be utilized for simulating how different geophysical variables translate to spectral radiance, and how the medium around it affects the values. It is also useful for simulating how the atmosphere affects the radiance values for various wavelengths, angles and weather. Improved trade-off studies in payload design would be possible by simulating the TOA radiometry reaching a detector.

The resulting radiance is higher when water clouds are present than when no clouds are present. The resulting water leaving radiance is almost identical regardless of whether it is computed by PlanarRad or by the lookup table. The temporal sensitivity analysis revealed that the longer the time period, the bigger the water leaving radiance variation.

The resulting radiance due to atmospheric effects with the solar zenith angle of 80° differs from other angles, both with regard to radiance at the surface and at TOA, by resulting in lower values. The solar zenith angles affect the water leaving radiance less than the solar azimuth angles do. The resulting radiance due to atmospheric effects are roughly the same regardless of viewing azimuth angle. The radiance due to atmospheric effects resulting from the viewing zenith angle of 60° is higher than for 30° and 0°, both at the ocean surface and at TOA. The resulting water leaving radiance values at the ocean surface differ significantly with regard to viewing zenith angles.

6. ACKNOWLEDGEMENTS

This work was supported by the Norwegian Research Council through the Centre of Autonomous Marine Operations and Systems (NTNU AMOS) (grant no. 223254), the MASSIVE project (grant

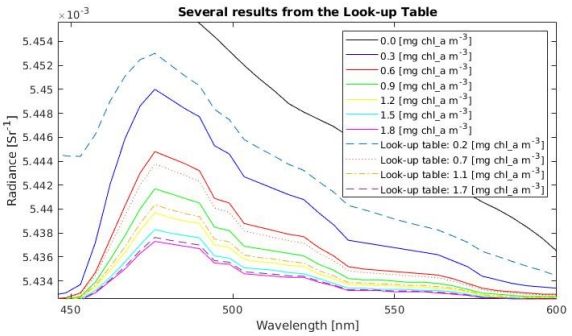

Fig. 5.

Water leaving radiance calculated by the lookup table and PlanarRad.

no. 270959).

We are grateful to Ingrid Ellingsen and SINTEF Ocean for assisting with the SINMOD simulation data.

7. REFERENCES

[1] Amir Ibrahim, Bryan Franz, Ziauddin Ahmad, Richard Healy, Kirk Knobelspiesse, Bo-Cai Gao, Chris Proctor, and Peng-Wang Zhai. Atmospheric correction for hyperspectral ocean color retrieval with application to the hyperspectral imager for the coastal ocean (hico). *Remote Sensing of Environment*, 204:60–75, 2018.

[2] Joseph D Ortiz, Dulci M Avouris, Stephen J Schiller, Jeffrey C Luvall, John D Lekki, Roger P Tokars, Robert C Anderson, Robert Shuchman, Michael Sayers, and Richard Becker. Evaluating visible derivative spectroscopy by varimax-rotated, principal component analysis of aerial hyperspectral images from the western basin of lake erie. *Journal of Great Lakes Research*, 2019.

[3] M Guelman and F Ortenberg. Small satellite's role in future hyperspectral earth observation missions. *Acta Astronautica*, 64(11):1252–1263, 2009.

[4] Darryl J. Keith, Blake A. Schaeffer, Ross S. Lunetta, Richard W. Gould Jr., Kenneth Rocha, and Donald J. Cobb. Remote sensing of selected water-quality indicators with the hyperspectral imager for the coastal ocean (hico) sensor. *International Journal of Remote Sensing*, 35(9):2927–2962, 2014.

[5] M. Soukup, J. Gailas, D. Fantin, A. Jochemsen, C. Aas, P. J. Baeck, L. Benhadj, S. Livens, B. Delauré, M. Menenti, B. G. H. Gorte, S. E. Aria Hosseini, M. Esposito, and C. N. van Dijk. Hyperscout: Onboard processing of hyperspectral imaging data on a nanosatellite. In *Small Satellites, System and Services Symposium (4S), Valletta, Malta*, 2016.

[6] Curtis Mobley. Ocean optics web book.

[7] F. Sigernes. Basic hyperspectral imaging. *TTK20 Hyperspectral remote sensing - lecture notes, Norwegian University of Science and Technology, Trondheim*.

[8] Dag Slagstad and Thomas A. McClimans. Modeling the ecosystem dynamics of the Barents Sea including the marginal ice zone: I. Physical and chemical oceanography. *Journal of Marine Systems*, 58(1-2):1–18, October 2005.

[9] Paul Wassmann, Dag Slagstad, Christian Wexels Riser, and Marit Reigstad. Modelling the ecosystem dynamics of the Barents Sea including the marginal ice zone: II. Carbon flux and interannual variability. *Journal of Marine Systems*, 59(1-2):1–24, January 2006.

[10] Dick P Dee, SM Uppala, AJ Simmons, Paul Berrisford, P Poli, S Kobayashi, U Andrae, MA Balmaseda, G Balsamo, d P Bauer, et al. The era-interim reanalysis: Configuration and performance of the data assimilation system. *Quarterly Journal of the royal meteorological society*, 137(656):553–597, 2011.

[11] Gary Egbert and Lana Erofeeva. The osu topex/poseidon global inverse solution tpxo.

[12] Jon Hedley. A three-dimensional radiative transfer model for shallow water environments. *Optics Express 16*.

[13] John Hedley. Planarrad result sheet for hydrolight comparison.

[14] Zhonghai Jin. A note on coart and its input.

[15] John Hedley. Brdf of a material with isotropic phase function.

[16] Zhonghai Jin. View geometry web.